LAWRENCE LIVERMORE NATIONAL LABORATORY

LLNL-JRNL-667942

An analysis of methods of determining the effective eddy viscosity of an Implicit LES for mixing simulations

Y. Zhou, B. Thornber

March 3, 2015

ASME J Fluids Engineering

An analysis of methods of determining the effective eddy viscosity of an Implicit LES for mixing simulations

Ye Zhou

Lawrence Livermore National Laboratory

Livermore, CA 94550, USA

Ben Thornber

School of Aerospace, Mechanical and Mechatronic Engineering

The University of Sydney

NSW 2006, Sydney, Australia

ABSTRACT

The Implicit large-eddy simulations (ILES) have been utilized as an effective approach for calculating many complex flows at high Reynolds number flows. Richtmyer–Meshkov (RM) instability induced flow can be viewed as a homogeneous decaying turbulence (HDT) after the passage of the shock. In this article, a critical evaluation of three methods for estimating the effective Reynolds number and the effective kinematic viscosity is undertaken utilizing high resolution ILES data. Effective Reynolds numbers based on the vorticity and kinetic energy decay rate, or the integral length and dissipation scale are found to be the most self-consistent when compared to the expected phenomenology and wind tunnel experiments.

1. Introduction

The Richtmyer–Meshkov instability (RMI) [1,2] induced turbulent fluids have important scientific and engineering applications. These instability driven fluids have found applications [3-6] in astrophysical flows and inertial confinement fusion. Recently, Implicit large-eddy simulations (ILES) [7] have demonstrated as an effective approach for calculating high Reynolds number flows one frequent encountered in scientific and engineering applications.

Because the subgrid scale modeling is provided implicitly by the numerics, the ILES methodology posed a challenge [8] when one is interested in the Reynolds number (Re) of the flows,

$$Re = UL/\nu_0. \qquad (1)$$

In the ILES framework, the effective kinematic viscosity, ν_0, is not available. *U* and *L* are the characteristic velocity field and length scale, respectively, and both quantities are dominated by the large-scale properties and are readily obtained from the simulated data. It should be noted that in large-eddy simulations (LES), a subgrid model is employed instead [9]. We will come back to this point later.

The RMI induced turbulent flow can be viewed as a freely decaying, incompressible one after the passage of the planar shock wave [10] (see also, references [11-12]). Without other energy deposition, the energy balance equation is reduced to a decaying one. Freeing from the external agencies (see for example, references [13-14]), homogeneous decaying turbulence (HDT) offered a clean platform to study issues of concerns for the RMI flows.

This paper will explore three schemes for evaluating the effective eddy viscosity which gives an important guide to the fidelity of mixing simulations, utilizing an ILES algorithm [31-34,38-40] which has been employed previously for RM calculations. We will inspect three proposed methods of computing *Re*.

2. Effective viscosity and Reynolds number

As noted in Ref. [8], the strength of LES is its potential for capturing the high Re turbulent flows. Therefore, there is no need at all to pay attention to these flows where the values of *Re* are clearly low. These low Re flows should be handled accurately with direct numerical simulations (DNS) [16] and can be identified easily by their lacking of a scale separation between the energy containing and dissipation regions [17,18]. Therefore, this paper will only focus on the applications where an extended inertial range can be illustrated using the simulation datasets.

Recall that the dynamics of the turbulent flows is governed by the time-dependent evolution of large-scale, energy-containing scales [17, 18]. In the Kolmogorov theory, the constant energy flux across a scale k is the only link between the energetic and dissipation scales [19, 20]. A suitable analogy [see Fig. 17, Ref. 20] for an extended inertial range is a long "pipe" without leaks. We can "cut" a finite section from this "pipe" and view its inflow and outflow.

Within the ILES framework, the energy flux, ε, can be evaluated from the energetic scales of the flows as the energy input into the upper bound of the inertial range. For forced turbulent flow, for example, the inflow of the energy can be simply obtained by the forcing correlation functions at the large scales [8, 21]. For complex flows, the energy inflow may be modeled from [18]

$$\varepsilon = D_\infty U^3/L. \qquad (2)$$

The coefficient approaches a constant value of $D_\infty \approx 0.5$ for the high Reynolds number flow where an internal range has been established [22,23].

The outflow of the energy from the lower bound of the inertial range would correspond to the dissipation [18]. In direct numerical simulations, the energy flux is defined as

$$\varepsilon \equiv \int_0^{Kd} 2\nu_0 k^2 E(k)\,dk \qquad (3)$$

Here $K_d = 2\pi/\eta$ is the Kolmogorov wavenumber, where $\eta_K = \nu_0^{3/4}/\varepsilon^{1/4}$ is the Kolmogorov length scale.

In ILES calculations of high Reynolds number flows, the Kolmogorov wavenumber can't be resolved. Yet, the highest resolvable wavenumber of ILES, saying k^* ($k^* < k_d$), is known. The effective viscosity, ν_{eff}, can then be defined as

$$\varepsilon = \left[\int_0^{k^*} + \int_{k^*}^{kd}\right] 2\nu_0 k^2 E(k)\,dk = \int_0^{k^*} 2\nu_{eff} k^2 E(k)\,dk = \nu_{eff}\Omega \qquad (4)$$

where the enstrophy, Ω, is given in ILES by

$$\Omega = \int_0^{k^*} 2k^2 E(k)\,dk. \qquad (5)$$

In this fashion, we are attempting to partition the energy outflow (which equals to the energy flux) into two distinctive elements. First, the enstrophy contains the contributions from all of the eddies of the ILES resolvable scales. On the other hand, for those eddies with their scales smaller than $\eta^* = 2\pi/k^*$, the effective viscosity defined above incorporates the collective dissipative effects of those unresolvable scales. Of course, the influences of the numerical dissipations are expected, but as $k^* \rightarrow k_d$, the value of the effective viscosity decreases ($\nu_{eff} \rightarrow \nu_0$).

In the physical space, the smallest length scale that one should employ should be η^*, and ν_{eff} can be written as [12],

$$\nu_{eff} = \varepsilon/\Omega \qquad (6)$$

where $\Omega = \overline{\omega^2}/2,$ in the physical space, where the vorticity, ω, can be readily evaluated based on the simulated velocity data.

Restricting to HDT, the energy balance equation takes its simplest form (Eqn. (106) of Ref. 24)

$$\frac{dK(k)}{dt} = -\varepsilon = -\nu_{eff}\Omega \qquad (7)$$

or

$$\nu_{eff} = -\frac{dK(k)}{dt} \Big/ \Omega \qquad (8)$$

The decay energy equation can be non-dimensionalized using

$$t^* = t(\frac{U}{L}), \qquad (9a)$$

and

$$K^* = \frac{K}{U^2}. \qquad (9b)$$

The effective Re_{eff} is then obtained from the definition

Re_{eff} = -Ω* /(dK*/dt*). (10)

The above procedure can also be justified from the LES perspective. For simplicity, the classical Heisenberg model (see, for example, [25] and [26])

$$\varepsilon = 2\nu_t \int_0^{kc} k^2 E(k)dk \qquad (11)$$

is an earliest spectral subgrid model for large-eddy simulations, where k_c is the cutoff wavenumber of the LES and ν_t is the turbulent viscosity. As noted in [26], the Heisenberg model has an assumption which effectively gives an average of the effect of both local and non-local interactions but with more weight given to the non-local interactions. Therefore, the effective viscosity estimation for an ILES summarized in this section can be interpreted as a method of reverse engineering, which allows us to reconstruct what would be Heisenberg turbulent viscosity of a LES, if the cutoff wavenumber k_c is always dynamically chosen at the highest resolved ILES wavenumber, k*. Also, the above discussion is also relevant with the previous evaluation [15] of the spectral eddy viscosity of Chollet [27] for a HDT flow (for a detailed review on using statistical approaches to deriving the formulations of spectral eddy viscosity, see [14]).

3. Three proposed models

In this section, we will restrict ourselves to the cases where an inertial range has been achieved in an ILES. It is reasonable to assume that the extent of the inertial range corresponds to how high the Reynolds number has been achieved.

The existence of an extended inertial range would provide some opportunities to estimate the effective kinematic viscosity [8]. It also made it possible to argue that the energy-containing scale is free from the numerical dissipation scale, which is grid dependent. This section addresses the following question: For a flow field computed from a highest resolution ILES, what is the best estimation of the corresponding Reynolds number from either a DNS or experiment that would be able to produce the same energy-containing scale dynamics or the extent of the inertial range? Once this Reynolds number can be obtained, the effective kinematic viscosity is followed.

The first method of computing the effective Reynolds utilizes the enstrophy and decay rate as detailed in Eqn. (11). The second proposed method utilizes our knowledge of the lower boundary of the inertial range (assuming a dissipative scheme), the inner viscous length scale [9,20], is given by

$\lambda_v = 50\ \delta\ \mathrm{Re}^{-3/4}$. (12)

which can be easily rearranged to give the Reynolds number.

Finally, the third method explores the use of the Liepmann-Taylor length scale to determine the effective Re. The Liepmann-Taylor length scale, $\lambda_{L\text{-}T}$, is the boundary between the energy-containing and inertial ranges is given by the (see for example, [29] and [30])

$$\lambda_{L\text{-}T} = 5\ \delta\ Re^{-1/2} \qquad (13)$$

where δ is the outer length scale of the flow. For a given ILES, it is reasonable to expect that such a boundary can be located and the value of λ_{L_T} should automatically reflect the dynamics of the energy-containing scales and length of the inertial range. In theory, λ_{L_T} could be determined by inspecting either the compensated energy spectra or the energy flux function. In practice, however, the visual inspection process of this value is a challenge, and it is actually easier to compute it indirectly from the Taylor microscale, λ_T. Using the jet experimental data [29],

$$\lambda_{L\text{-}T} \sim 2.17\ \lambda_T\ . \qquad (14)$$

The coefficient on the right hand side of Eqn. (14) might not be universal and it is highly desirable to calibrate it using other experimental datasets. If the outer scale δ is available, the Reynolds number can be simply determined with two large-scale length scales,

$$\mathrm{Re} = [5\delta/\lambda_{L\text{-}T}]^2. \qquad (15)$$

Hence, the third method explored which is based on the inertial range information only is to determine the Reynolds number, from the following

$$Re=[10\lambda_{L\text{-}T}/\lambda_\nu]^4. \qquad (16)$$

For both Eqns. (12) and (16), the effective kinematic viscosity could be simply obtained by

$$\nu_{eff} = UL/\mathrm{Re}, \qquad (17)$$

where once again, *U, L* are large-scale measurements.

4. Numerical testing

The proposed methods of computing an effective Reynolds number have been tested numerically. Simulations of homogeneous decaying turbulence were undertaken using a high order accurate Implicit LES algorithm [15, 31-34] at grid resolutions up to 1024^3. The simulations utilized the initial conditions previously employed by Thornber et al. [15], except adapted to initialize the peak of the kinetic energy spectrum k_p=32, permitting a range of large and small length scales. The large scales are initialized with a k^4 spectrum and the small scales have an exponential drop-off. The simulations were run to late non-dimensional time τ=t k_p u_{rms}(t=0)=1000 to allow the turbulent flow field to develop.

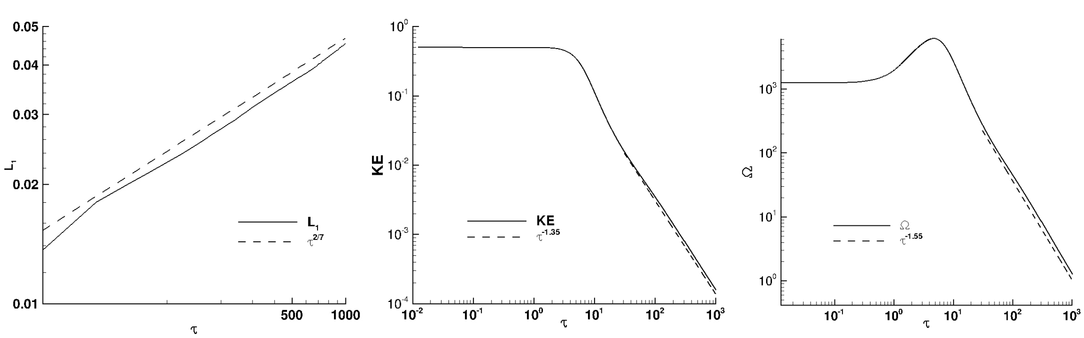

Fig. 1

a. Time variation of integral length (left), *b. turbulent kinetic energy (middle)*

c. enstrophy (right)

First of all, Fig. 1 shows the time variation of the key properties of the flow field, namely the integral length L, the turbulent kinetic energy and the enstrophy. In classical scaling $L \sim t^{2/7}$ and this scaling is shown to hold well at late times (Fig. 1a), where the virtual origin should have a reduced impact. The turbulent kinetic energy scales $\sim t^{-10/7}$, here we find a close fit to a slightly smaller exponent of $t^{-1.35}$ (Fig. 1b).

For the evolution of enstrophy, a simple model can hint at the expected time variation.

$$\Omega = \int_0^{k_L} E(k < k_L) k^2 dk + \int_{k_L}^{k_v} E(k > k_L) k^2 dk$$

Assuming k^4 at the low wavenumbers and $k^{-5/3}$ at the high wavenumbers, joining at $k_L=2\pi/L$, and noting that $k_L \sim t^{-2/7}$ and that in the case presented here $k_v/k_L \sim 10$ leads to the result that $\Omega \sim t^{-12/7}$. Any k^2 component at low wavenumber would modify this to be $t^{-8/7}$. In Fig. 1c the enstrophy scales as $\sim t^{-1.55}$ which is marginally lower than $-12/7 \sim -1.71$. Finally, the skewness of the velocity derivative structure function is -0.38 (not shown), indicative of a non-Gaussian turbulent field [35].

Fig. 2 shows the spectra from the current simulations at several different time instants. Two comments must be made here, the first is that the apparent sub-inertial range exhibits a bottle-neck as would be expected in decaying homogeneous cases, or moderate Reynolds number grid generated turbulence. This leads to an inertial exponent approximately $k^{-1.5}$ which is the same as measured in recent active grid experiments by Thormann and Meneveau [36] (Fig. 17) at Re_λ approximately the same as reported here. Their results also have a similar length of the sub-inertial range. The results shown here indicate that a sensible choice of λ_v is at k~100, where rapid viscous decay begins.

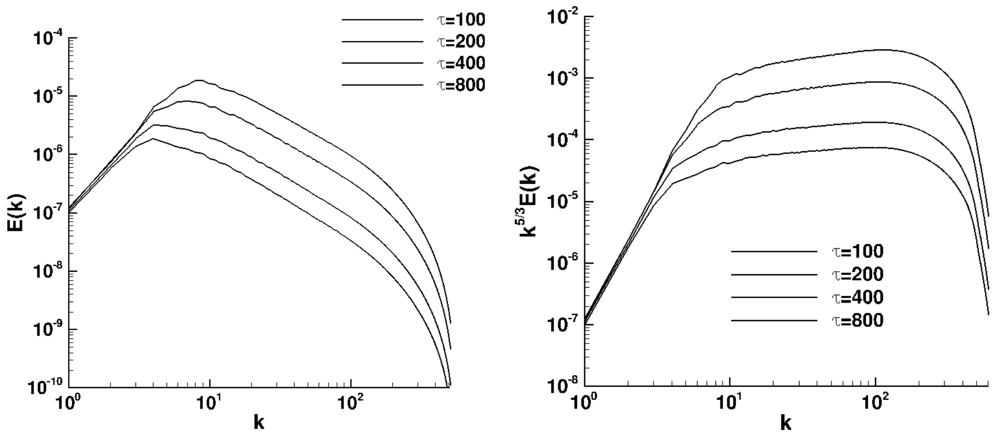

Fig 2 Turbulent kinetic energy spectra and compensated spectra as a function of time

This high resolution data was then employed to calculate the Reynolds number based on Eqn. (11), Eqn. (12) and Eqn (16). Based on the previous expected time dependencies, the Reynolds number dependence on time during the simulation can be predicted. Assuming that λ_v is fixed by the grid spacing, as will be verified later, then:

$$Re\ (\Omega) = \frac{u\,L\ \ \Omega}{\epsilon} \propto \frac{t^{-5/7}\ t^{2/7} t^{-12/7}}{t^{-17/7}} \propto t^{2/7} \quad (18)$$

$$Re\ (L\ \ ) = \left(\frac{\lambda_v}{50L_1}\right)^{-4/3} \propto t^{8/21} \qquad (19)$$

$$Re(\lambda_{L-T}) = Re\ (\lambda_T) = \left(\frac{10\lambda_{L-T}}{\lambda_v}\right)^4 = \left(\frac{21.7\lambda_T}{\lambda_v}\right)^4 \propto t^2 \quad (20)$$

The first two relations give reasonably close time dependence of Re, however the latter is very difference thanks to the strong scaling of $\lambda_T \sim t^{1/2}$. These time dependencies give a useful sanity check to the performance of the numerical schemes.

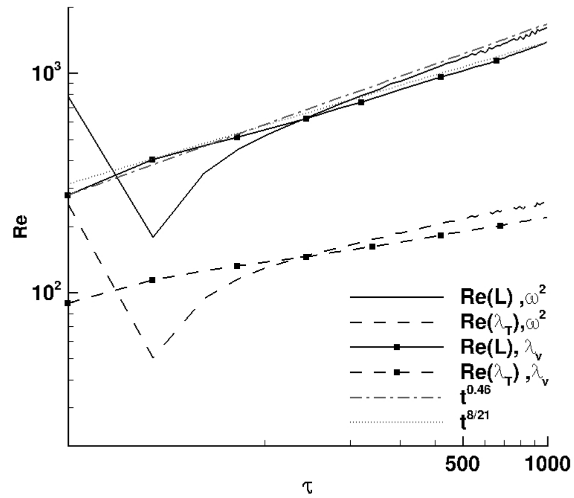

Fig 3. Effective Reynolds number

Figure 3 plots both the Reynolds number based on the Taylor micro-scale (average over the three directions) and the integral length, where the integral length is calculated from the intercept of the kinetic energy spectrum. At the latest time Re ~250 and Re~1600. There is a reasonable level of consistency between the two approaches, despite the theoretically predicted small difference in the time exponent. In the simulation the scaling of Reynolds based on Eqn. (12) with time is as predicted, but for the method based on enstrophy it is marginally higher at $t^{0.46}$. This is due to the slight differences in time scaling of enstrophy and kinetic energy compared to the idealized Kolmogorov model.

A common assumption is that $Re_L \approx C\,(Re_\lambda)^2$ [29, 30, 8] (where C is a constant), however at these grid resolutions this clearly does not hold. Fig 4 plots the two length scales, normalized by the box width. The relationship is clearly nonlinear, where L~3 λ_T at early time and L~7 λ_T at the final time, however it is not yet sufficiently non-linear to justify the above relationship, hence such an estimation is optimistic at low separation lengthscales (the constant in front of the proportionality must be employed).

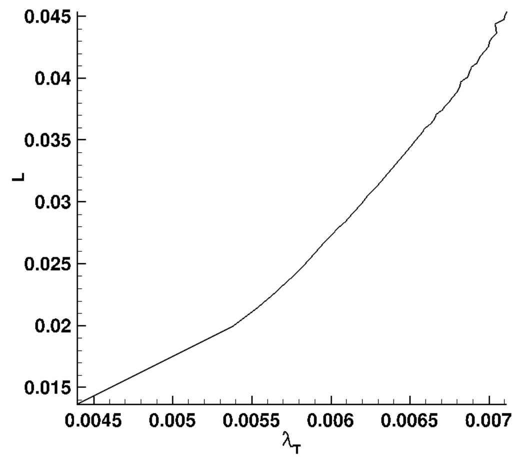

Fig. 4 Integral length plotted against the Taylor microscale for the duration of the simulation

The two eddy viscosities are plotted in Fig 5. As expected from the Reynolds number plots, the eddy viscosities also agree well taking a value of ~2.5 x 10^{-7} at late times. The ideal expected time variation of effective viscosities are $t^{-17/21}$ for the method based on the inner viscous scale, and $t^{-5/7}$ for the enstrophy based effective viscosity. The results match these predictions closely, accounting for the observed scaling of kinetic energy.

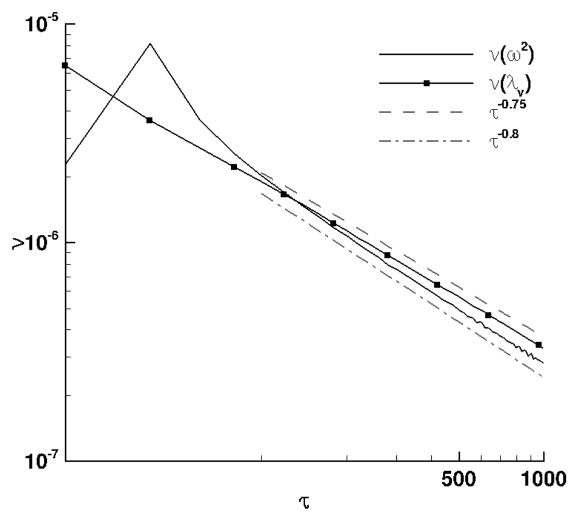

Fig. 5. Eddy viscosities computed using Eqn (11) and (12)+(17) respectively.

Finally an assessment of Reynolds number was made using Eqn. (16). From the functional form it is very sensitive to the ratio of the length scales. However, determining λ_{L-T} accurately from the spectra alone is not simple. For example, assuming that λ_{L-T} k=20 at the final grid resolution gives a Reynolds number of $7x10^6$, significantly higher than any of the estimates from the previous equations. Raising the ratio of the length scales to the fourth power means that an accurate determination is required which is perhaps beyond simple eye-balling. Assuming that the correlation λ_{L-T} ~2.17 λ_T from turbulent jet data holds here, the computation of the Reynolds number can be automated. The results of this are shown in Figure 6. Again, the predictions are substantially higher than the previous two methods.

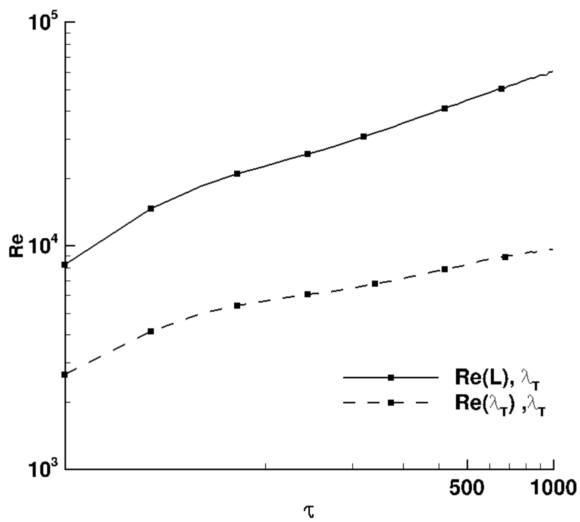

Fig 6 Effective Reynolds number based on the Taylor micro-scale and inner viscous scale.

5. Summary

The goal of this work is to further develop and evaluate the methodologies for obtaining the effective Reynolds number and viscosity, both of these measurements are important guide to the fidelity of mixing computations using implicit large-eddy simulations (ILES). Recently, this task takes a greater urgency as ILES has demonstrated its utility for computing complex flows of interest; such as the Richtmyer-Meshkov (RM) as well as the Rayleigh-Taylor instabilities[1] induced flows. Focusing on high Reynolds number turbulent flows, we have formulated three schemes for achieving this objective. These proposals have been test numerically in order to determine their performance in an ILES setting. Simulated flow fields of the homogeneous decaying turbulence (HDT), computed with an ILES code which has been employed previously for RM calculations, have been employed. It should be noted that the RMI induced turbulent flow can be viewed as a freely decaying, incompressible one after the passage of the planar shock wave.

Based on our observations, it can only be concluded that if high Reynolds number effects, such as increased intermittency and mixing transitions at the grid scale, are important then the most reliable approach and most widespread is the calculation of the effective Reynolds based on the enstrophy or on the inner viscous scale and the integral length. These measures of Reynolds appear the most consistent with the observed behavior of the flow field.

ACKNOWLEDGMENT

This work was performed under the auspices of the Lawrence Livermore National Security, LLC under Contract No. DE-AC52-07NA27344. This research was supported under Australian Research Council's Discovery Projects funding scheme (project number DP150101059). The authors would like to acknowledge the computational resources at the National Computational Infrastructure through the National Computational Merit Allocation Scheme which were employed for all cases presented here.

[1] For a recent example, see Ref. 37

REFERENCES

[1] Richtmyer, R.D., 1960 ''Taylor instability in shock acceleration of compressible fluids,'' Commun. Pure Appl. Math. **13**, 297.

[2] Meshkov, E.E., 1969 "Instability of the interface of two gas accelerated by a shock wave," Izv., Acad. Sci., USSR Fluid Dyn. 4, 101

[3] Muller, E., B. Fryxell, and D. Arnett, 1991 Instability and clumping in SN 1987A, Astron. Astrophys. **564**, 896.

[4] Lindl, J., 1998, Inertial Confinement Fusion: The Quest for Ignition and Energy Gain Using Indrect Drive, AIP Press, New York

[5] Zhou, Y. et al., 2003. Progress in understanding turbulent mixing induced by Rayleigh–Taylor and Richtmyer–Meshkov instabilities, Phys. Plasmas, **10**, 1883.

[6] Zhou, Y., Robey, H.F., and Buckingham, A.C., 2003. Onset of turbulence in accelerated high-Reynolds-number flow, Phys. Rev. E , **67**, 056305.

[7] Grinstein, F.F., Margolin, L.G. and Rider, W.G., (Ed.), Implicit Large Eddy Simulation: Computing Turbulent Flow Dynamics (New York: Cambridge University Press), 2nd printing 2010.

[8] Zhou, Y., Grinstein, F.F., Wachtor, A.J., Haines, B.M. (2014). Estimating the effective reynolds number in implicit large eddy simulation, Phys. Rev. E , **89**, 013303.

[9] Sagaut, P., 2006. *Large Eddy Simulation for Incompressible Flows*, 3rd ed. (Springer,

Berlin).

[10] Zhou, Y., 2001, A scaling analysis of turbulent flows driven by Rayleigh–Taylor and Richtmyer–Meshkov instabilities, Phys. Fluids, 13, 538

[11] Clark, T.T., and Zhou, Y., 2006. Growth rate exponens of Richtmyer-Meshkov mixing layers, ASME J. Applied Mechanics, 73, 461

[12] Tritschler, V.K., Zubel, M., Hickel, S., and Adams, N. A., 2014. Evolution of length scales and statistics of Richtmyer-Meshkov instability from direct numerical simulations, Phys. Rev. E., 90, 063001

[13] Zhou, Y., Matthaeus, W. H., and Dmitruk, P., 2004. *Colloquium*: Magnetohydrodynamic turbulence and time scales in astrophysical and space plasmas, Rev. Mod. Phys. 76, 1065

[14] Zhou, Y., 2010. Renormalization group theory for fluid and plasma turbulence, Phys. Rep., 488, 1

[15] Thornber B, Mosedale, A. Drikakis D, 2007. On the Implicit Large Eddy Simulation of Homogeneous Decaying Turbulence, J. Comput. Phys., 226, 1902

[16] Moin, P., and Mahesh, K., 1998. Direct numerical simulation: A tool in turbulence research, Annu. Rev. Fluid Mech., 30, 539

[17] Tennekes, H., and Lumley, J.L., First Course in Turbulence (MIT Press, Cambridge, MA, 1972)

[18] Batchelor, G.K., The theory of homogeneous turbulence, (Cambridge University Press, Cambridge, UK, 1953)

[19] Zhou, Y., 1993. Degree of locality of energy transfer in the inertial range, Phys. Fluids A, 5, 1092

[20] Zhou, Y., 1993. Interacting scales and energy transfer in isotropic turbulence, Phys. of Fluids A, 5, 2511.

[21] Fureby, C., and Grinstein, F.F., Monotonically integrated large eddy simulation of free shear flows, AIAA J. **37**, 544 (1999).

[22] Sreenivasan, K.R., 1998, An update on the energy dissipation rate in isotropic turbulence, Phys. Fluids, **10**, 528.

[23] Keneda, Y., T.Ishihara, M. Yokokawa, K. Itakura, and A. Uno, “Energy dissipation rate and energy spectrum in high resolution direct numerical simulations of turbulence in a periodic box,” Phys. Fluids, **15**, L21 (2003).

[24] Zhou, Y. and Speziale, C.G., 1998. Advances in the fundamental aspects of turbulence: Energy transfer, interacting scales, and self-preservation in isotropic decay, ASME Appl. Mech. Rev., 51, 267

[25] Monin, A.S., and Yaglom, A.M., Statistical fluid mechanics: mechanics of turbulence, Vol 2 (MIT Press, Cambridge, MA, 1975)

[26] Bataille, F., Rubinstein, R., Hussaini, M.Y., 2005, Eddy viscosity and diffusivity modeling, Physics Letters A 346, 168

[27] Chollet, J., Turbulent Shear Flows IV, Springer-Verlag, 1984, pp. 62–72 (Chapter: Two-point closures as a subgrid-scale modelling tool for large eddy simulations).

[29] Dimontakis, P.E., 2000. The mixing transition in turbulent flows, J. Fluid Mech., 409, 69

[30] Zhou, Y., 2007, Unification and extension of the concepts of similarity criteria and mixing transition for studying astrophysics using high energy density laboratory experiments or numerical simulations, Phys. Plasmas, **14**, 082701.

[31] Thornber, B., Zhou, Y. (2012). Energy transfer in the Richtmyer-Meshkov instability. *Physical Review E*, 86, 056302.

[32] Garcia-Uceda Juarez, A., Raimo, A., Shapiro, E., Thornber, B. (2014). Steady Turbulent Flow Computations Using a Low Mach Fully Compressible Scheme. *AIAA Journal*, 52, 2559.

[33] Shanmuganathan, S., Youngs, D., Griffond, J., Thornber, B., Williams, R. (2014). Accuracy of high-order density-based compressible methods in low Mach vortical flows. *International Journal for Numerical Methods in Fluids*, 74, 335

[34] Probyn, M., Thornber, B., Drikakis, D., Youngs, D., Williams, R. (2014). An Investigation into Non-Linear Growth Rate of Two-Dimensional and Three-Dimensional Single-Mode Richtmyer-Meshkov Instability using an Arbitrary-Lagrangian-Eulerian Algorithm. ASME *Journal of Fluids Engineering*, 136(9), 091208

[35] Sreenivasan, K.R., and Antonia, R.A., 1997. The phenomenology of small-scale turbulence, Annu Rev. Fluid Mech., 29, 435

[36] Thormann, A. and Meneveau, C., 2014. Decay of homogeneous, nearly isotropic turbulence behind active fractal grids, Phys. Fluids, 26, 025112

[37] Andrews, M.J., Youngs, D.L., Livescu, D., and Wei, T., 2014. Computational studies of two-dimensional Rayleigh-Taylor driven mixing for a tilted-rig. ASME *Journal of Fluids Engineering*, 136(9), 091212

[38] Thornber B, Drikakis D, Williams RJR & Youngs D, 'An Improved Reconstruction Method of Compressible Flows with Low Mach Number Features' , J. Comput. Phys., 227 (10) 4853-4872, 2008.

[39] Thornber B, Drikakis D, Youngs DL & Williams RJR , 'The influence of initial conditions on turbulent mixing due to Richtmyer-Meshkov instability' J. Fluid Mech., 654 99-139, 2010.
[40] Thornber B, Drikakis D, Youngs DL & Williams RJR , `Growth of a Richtmyer-Meshkov turbulent layer after reshock' , Phys. Fluids, 23 (9) 095107-1-095107-15, 2011.